Optimizing Virtual Classrooms: Real-Time Emotion Recognition with AI and Facial Features

Abdelhak Sakhi [a,1], Salah-Eddine Mansour [a,2,*]

[a] Department of Computer Science, Faculty of Sciences Ain-Chock, Hassan II University, Casablanca, Morocco
[1] abdelhak.sakhi-etu@etu.univh2c.ma; [2] salaheddine.mansour-etu@etu.univh2c.ma
* Corresponding Author

ARTICLE INFO	ABSTRACT

Online education, especially post-COVID, faces the challenge of maintaining student engagement, particularly at the college level. A key factor in effective learning is understanding students' emotional states, as they influence comprehension and participation. To address this, we propose an intelligent system that classifies students' emotions by analyzing facial expressions, allowing teachers to adapt their methods in real-time. Our system utilizes the Learning Focal Point algorithm to improve emotion classification accuracy, focusing on key facial regions related to emotional expressions. The methodology involves preprocessing facial images, extracting features, and classifying emotions using the algorithm. Trained on a diverse dataset, the system performs well under various conditions, with a classification accuracy of 94% based on a well-known database. Although the system shows significant improvements over traditional methods, factors like image quality and internet connection can impact accuracy in real-world applications. Ultimately, our approach enhances remote learning by providing real-time emotional feedback, fostering a more responsive and student-centered environment.

1. Introduction

The growth of online education, particularly following the COVID-19 pandemic, has reshaped how learning is delivered. While remote learning provides flexibility and accessibility, it also brings challenges in sustaining student engagement and ensuring effective teaching. A key issue is the difficulty in gauging students' emotional states, which significantly impact their learning experience. Unlike in traditional classrooms, where teachers can observe body language and facial expressions, remote education restricts these visual cues, making it harder to adjust teaching methods in real-time [1]–[3].

To address this challenge, integrating AI-driven emotion classification systems into virtual classrooms can help teachers better understand student engagement and learning difficulties. By analyzing facial expressions, AI can classify emotions and provide real-time feedback, enabling educators to adjust their teaching methods accordingly. However, this solution is not yet supported by popular platforms like Microsoft Teams or Google Meet. Our vision is to integrate this solution into these applications using their APIs, allowing users to benefit from both solutions. This approach enhances remote learning by creating a more interactive and adaptive educational environment [4], [5].

In order to safeguard student privacy and avoid potential misinterpretation of individual emotions, our solution provides only aggregated emotion data for the entire classroom. Professors will not see the specific emotional states of individual students. Instead, they will receive global statistics that reflect the overall emotional mood or engagement level of the class. This ensures that students' privacy is maintained while still offering useful insights into the classroom's emotional dynamics. By focusing on class-wide trends, educators can adjust their teaching methods based on the general emotional state of the group, creating a more adaptive and responsive learning environment.

Recent studies have explored facial expression recognition to monitor student progress in online education. By using ResNet-50 for feature extraction and a convolutional attention mechanism, one approach achieved 87.62% and 88.13% accuracy on the RAF-DB and FER2013 datasets. These advancements demonstrate the effectiveness of AI-driven emotion detection in enhancing teaching methods and improving student engagement [7]–[9].

Understanding student emotions is vital for improving engagement in virtual education. Existing systems like Affectiva and Emotient face integration challenges on platforms like Microsoft Teams. This study presents a Teams-based system using speech and facial emotion detection with TensorFlow, PyTorch, and OpenCV, achieving 95% precision for positive emotions. While engagement improved, further work is needed to detect complex emotions such as stress and frustration [10]–[12].

Recent research on emotion classification using EEG data focuses on dry electrodes, machine learning, and brain-computer interfaces. This study compares three EEG features, introduces feature smoothing to reduce noise, and uses manifold learning to track emotion changes. Results show that power spectrum features perform best, smoothing improves accuracy, and emotion trajectories can be visualized [13], [14].

As we can observe, there has been considerable research on emotion classification, with various methods proposed to improve the accuracy and effectiveness of emotional state detection. However, most of these approaches do not utilize our proposed method, the Learning Focal Point (LFP) algorithm. Unlike traditional methods, which rely on standard machine learning techniques or existing deep learning models, the LFP algorithm focuses on enhancing precision by effectively identifying key features within the emotional data. By applying this method, we have achieved a remarkable accuracy of 94%. The unique structure of LFP enables it to optimize the classification process, distinguishing emotional states with greater accuracy and providing more reliable real-time feedback. This demonstrates the potential of LFP to outperform existing methods and significantly advance the field of emotion classification [15]–[17]. This article presents the proposed method, the Learning Focal Point (LFP) algorithm, followed by the results and discussion section, where its performance is compared to traditional methods. The conclusion summarizes the findings and explores future applications, particularly in emotion detection for online education.

2. The Proposed Method

2.1. Dataset

The dataset used in this study is from the "Representation Learning Challenges: Facial Expression Recognition (FER) Challenge" on Kaggle. The main objective of this challenge is to classify facial expressions into various emotion categories, which is critical for applications such as emotion recognition in human-computer interaction and affective computing. The dataset typically consists of images that are labeled with one of several distinct emotion categories, including happiness, sadness, anger, surprise, fear, disgust, and neutral. For our work, we leveraged this dataset to train our neural network model [18]–[20].

Specifically, we utilized the "Facial Expression Recognition 2013 (FER2013)" dataset, which is commonly used in facial expression recognition tasks. This dataset contains 48×48-pixel grayscale

images of human faces, where each image is associated with one of seven emotion labels. The FER2013 dataset includes approximately 35,000 images, categorized into seven different emotional states, providing a rich resource for training deep learning models to classify emotions accurately. By using this dataset, we were able to build and evaluate a robust model capable of detecting and classifying facial expressions in various emotional categories, ultimately improving the performance of our emotion recognition system [21], [22].

2.2. Research Design and Implementation

Our emotion classification system, which analyzes facial expressions to determine emotional states, consists of three primary modules, as illustrated in Fig. 1. The first module is responsible for detecting and tracking the student's face within video or image frames. It utilizes the OpenCV library, a powerful computer vision tool, to identify and locate the face in real-time, continuously tracking the face's position and movement across frames. This ensures that the facial features remain accurately identified, even when the student moves or changes facial expressions. The second module is based on the Learning Focal Point (LFP) algorithm, which enhances the system's ability to focus on the most relevant facial regions for emotion classification. By returning the coordinates of key areas such as the eyes, mouth, and eyebrows, the LFP algorithm extracts important facial regions that are critical for detecting emotions, filtering out irrelevant information and allowing the system to concentrate on expressive regions [23]–[26]. The third module calculates the weights of a neural network, which is trained to recognize different emotional states based on the identified facial features. Using these weights, the neural network classifies the facial expression into one of several emotion categories, such as happiness, sadness, anger, or surprise. Together, these three modules work seamlessly to provide an effective and efficient emotion classification system for various applications, such as online education or virtual interactions, see Fig. 1.
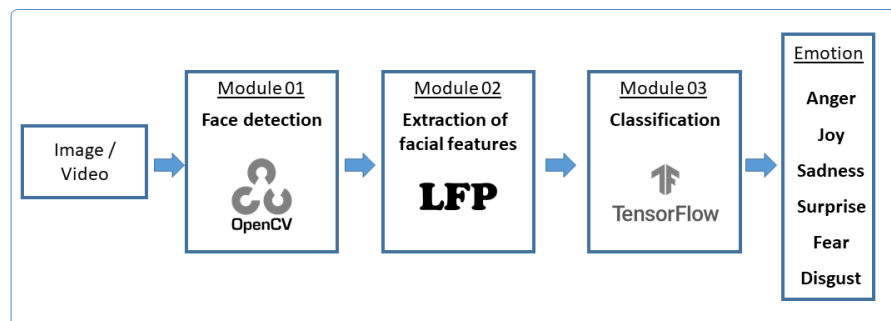

Fig. 1. System architecture for emotion classification based on facial expressionst

2.3. Method

In this paper, we have utilized the LFP Architecture, designed to enhance the efficiency and accuracy of data processing tasks. The architecture consists of three fundamental components: the LFP Algorithm, which serves as the foundational framework for data extraction and manipulation; the Selector, which aids in the precise identification and selection of relevant data subsets; and a dedicated block of neural networks, employed for advanced learning and processing tasks. Together, these components form a cohesive system that optimizes both data extraction and its subsequent analysis, contributing to the overall effectiveness of the methodology proposed in this study [27]–[29].

Our method is based on a novel concept centered around coordinates. Specifically, we partition each image into multiple sections and assign unique indices, referred to as coordinates, to each section. These coordinates are crucial as they guide the selector in extracting the most relevant pixel patches for analysis. As we see in the Fig. 2.
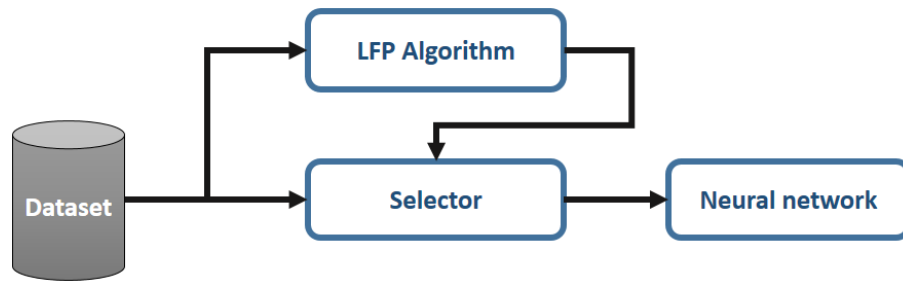
Fig. 2. Flowchart of the methodology using coordinate-based image partitioning

Our classification method uses the Learning Focal Point (LFP) algorithm to identify key regions in images for emotion recognition. Based on the Perceptron, LFP processes image datasets to highlight essential features like facial expressions and landmarks for accurate emotion classification. LFP then determines the coordinates of these critical regions, such as the eyes, mouth, and eyebrows, isolating the most relevant information for analysis and improving classification accuracy. The flowchart below (Fig. 3) illustrates the LFP algorithm's systematic approach to image analysis, feature extraction, and data processing, highlighting its efficiency in emotion classification.
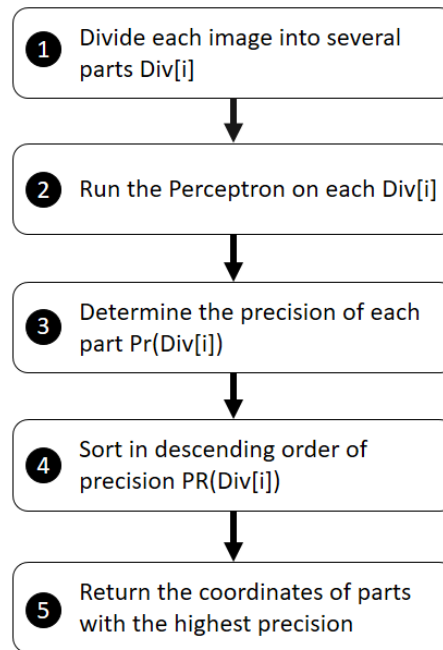

Fig. 3. Flowchart of the Learning Focal Point (LFP) algorithm: a visual guide to image analysis and feature extraction

The Learning Focal Point (LFP) algorithm starts by dividing each image in the dataset into distinct regions, creating smaller subdatasets, each with a unique coordinate index. This segmentation allows the algorithm to focus on specific parts of the image for targeted feature extraction [30], [31].

The algorithm then trains a perceptron model on each subdataset, allowing it to learn key patterns and features within the images. Afterward, the log-loss (a) is calculated for the training of each subdataset [32]–[34].

$$\text{Log-Loss} = -\frac{1}{N} \sum_{i=1}^{N} \sum_{c=1}^{C} y_{i,c} \log(p_{i,c}) \quad (a)$$

Finally, the algorithm identifies the subdataset with the lowest log-loss and returns its coordinates, highlighting key areas for emotion detection, such as facial features. This systematic approach ensures efficient feature extraction, laying a strong foundation for emotion classification [35], [36].

In conclusion, the Learning Focal Point (LFP) algorithm functions similarly to a pre-training step, enabling the calculation of Log-Loss by extracting the essential patches from the original data. What sets this method apart from others, such as Principal Component Analysis (PCA), is that instead of simply returning a reduced set of data or transformed features, the LFP algorithm identifies and provides the coordinates of the most critical patches within the data. This focus on the "effective" or key regions ensures that only the most relevant information is retained, which enhances the precision of emotion classification and feature extraction. Unlike methods like PCA, which may lose interpretability by compressing the data into abstract components, LFP directly highlights the significant regions for further analysis, making it a more targeted and effective approach [37]–[39].

In more detail, the LFP algorithm starts with a dataset where each row represents an image, including its pixel values and label, as shown in Fig. 4. It performs an initial estimation of latent factors, which are iteratively updated during training to improve accuracy until the model converges, ensuring precise predictions [40]–[42].

P1	....	P20	...	P40	...	P200	...	Y
210	...	67	...	27	...	54	...	1
231		157	...	113	...	23	...	0
...	....	...	...	...	...	...	...	...
224	....	77	....	50	....	54	...	2

Fig. 4. A dataset containing pixel values and target labels for each image: a comprehensive overview of image data representation

The first step in the Learning Focal Point (LFP) algorithm is to partition each image into distinct regions, as shown in Fig. 5. This segmentation divides the image into groups of columns, each with a unique coordinate index, allowing for more targeted analysis of key features. By organizing the image into smaller sections, the LFP algorithm focuses on the most relevant parts, improving feature extraction and classification accuracy.

Next, the LFP algorithm generates subdatasets by applying techniques like filtering or sampling to isolate important areas of the data. These subsets provide a refined view of the original dataset, allowing for more focused exploration of specific features or patterns. This approach enhances the flexibility of the analysis, as different subsets can be used to test various hypotheses, leading to more precise insights and robust conclusions. The process of creating and utilizing these subdatasets is visually illustrated in the Fig. 5, showcasing the segmentation and subsequent analysis [43], [44].

Each subdataset is individually trained using the perceptron model. This step is essential for enabling the perceptron to learn and identify the key features within the images that are crucial for accurate classification. Once the model has been trained, the Log-Loss is computed for each subdataset, and the coordinates with the minimum Log-Loss are selected [45].

The Selector block refines data extraction by using the coordinates identified by the Learning Focal Point (LFP) algorithm. These coordinates mark the most significant image regions, allowing the Selector to focus on specific pixel patches. This approach enhances computational efficiency by extracting only relevant visual information, reducing unnecessary data. After identifying key patches, the Selector further processes them to optimize feature extraction, improving the accuracy of

classification. By concentrating on critical areas, such as facial expressions or textures, the Selector maximizes the effectiveness of emotion classification. This process streamlines the data for deep learning tasks, as shown in Fig. 6, which illustrates how the Selector enhances input precision for final classification [46]–[48].
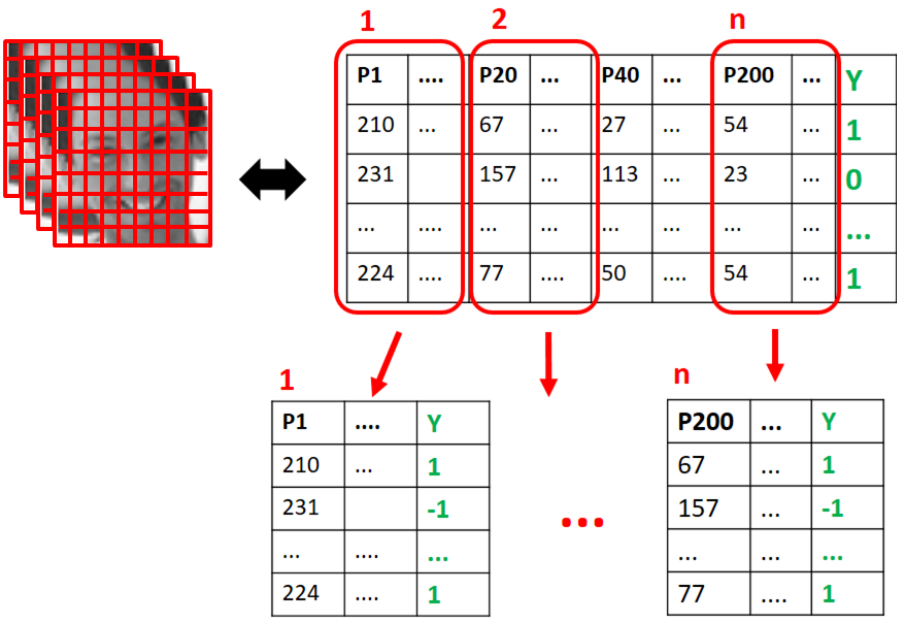

Fig. 5. Generating subdatasets for targeted data analysis and enhanced insights
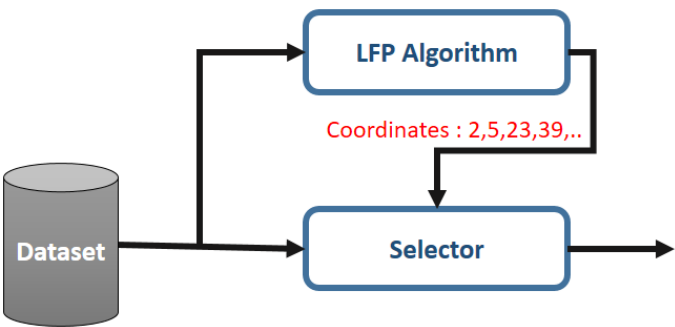

Fig. 6. Optimized extraction of relevant pixel patches through coordinate-guided selection in the LFP algorithm

The LFP algorithm is initially executed during the preprocessing stage to determine the foundational coordinates that guide the subsequent selection of crucial image regions. These coordinates serve as reference points for identifying the most relevant pixel patches within each image. However, unlike the LFP algorithm, which runs once during preprocessing, the Selector operates dynamically throughout both the training and testing phases. It continuously adapts to the current context, selecting the most informative pixel patches at each step of the learning process [49], [50]. This ensures that the model consistently utilizes the most relevant data points, enhancing its ability to extract meaningful features for classification. The dynamic nature of the Selector allows it to refine its selection iteratively, improving the efficiency and accuracy of both model training and evaluation. To demonstrate its effectiveness, we applied the LFP algorithm and Selector blocks to faces images, extracting essential pixels for further analysis, as illustrated in the Fig. 7.

Fig. 7. Workflow illustration of the selector during training and testing stages

The Selector is an algorithmic filter that extracts relevant pixel patches from an image based on coordinates, optimizing neural network performance by focusing on significant features. After applying the LFP algorithm, which identifies key feature points, the Selector filters out irrelevant pixels, ensuring only the most crucial information is retained. These selected pixel coordinates are passed to the neural network, allowing it to focus on relevant features during training and testing. This targeted approach improves efficiency, accuracy, and overall network performance in image processing tasks, as shown in Fig. 8.
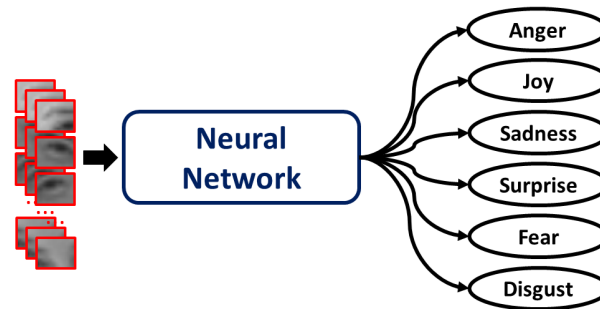

Fig. 8. Training and testing phases using the Multilayer Perceptron (MLP) neural network

We implemented a Multilayer Perceptron (MLP) neural network for learning, structured with four layers. The first layer consisted of 6,636 neurons, corresponding to the number of input pixels used for initial processing and feature extraction. The final layer was designed with six neurons, each corresponding to a specific emotion. To calculate the probability for each emotion, we employed the Softmax function, which enabled the network to output the likelihood for each emotional class.

3. Result and Discussion

After reviewing the methods employed in this research, we present the results obtained using the LFP algorithm and compare them with those from max pooling. The experiments were conducted using the Facial Expression Recognition (FER) challenge database available on Kaggle. Two experiments were performed, as shown in Fig. 6, to develop the models: in the first experiment, the LFP algorithm was applied in a convolutional neural network (CNN), and in the second experiment, max pooling was used. The performance of the models was evaluated using several metrics, including classification accuracy (CA), precision, recall, F1 score, and ROC-AUC values. These performance indices were automatically generated using the TensorFlow library [51]. Classification Accuracy (CA) is a fundamental metric in AI that measures how well the model performs by determining the proportion of correct predictions relative to the total number of predictions. It is defined as:

$$\text{Accuracy} = \frac{\text{TP} + \text{TN}}{\text{TP} + \text{TN} + \text{FP} + \text{FN}} \tag{1}$$

Where TP refers to True Positives, TN to True Negatives, FP to False Positives, and FN to False

Negatives. While accuracy is essential, it might not fully capture model performance, especially with imbalanced datasets, where it may be skewed by the majority class.

Precision is a metric used in classification tasks to measure the relevance of the positive predictions. It calculates the ratio of true positive predictions to the total number of predicted positives. The formula for precision is:

$$\text{Precision} = \frac{\text{TP}}{\text{TP} + \text{FP}} \tag{2}$$

A higher precision value indicates that the model is effective in making correct positive predictions, ensuring fewer false positives.

Recall, also known as sensitivity, measures the model's ability to identify all relevant instances within a dataset. It calculates the ratio of true positives to the sum of true positives and false negatives. The formula for recall is:

$$\text{Recall} = \frac{\text{TP}}{\text{TP} + \text{FN}} \tag{3}$$

A high recall indicates that the model captures most of the relevant instances, though it may include false positives [56].

The F1 score is a balanced measure that combines both precision and recall into a single value. It is particularly useful when class distributions are imbalanced. The F1 score is given by:

$$\text{F1 Score} = 2 \times \frac{\text{Precision} \times \text{Recall}}{\text{Precision} + \text{Recall}} \tag{4}$$

This score provides a comprehensive evaluation of the model's effectiveness by considering both false positives (precision) and false negatives (recall).

ROC-AUC (Receiver Operating Characteristic - Area Under the Curve) is a metric commonly used in binary classification to assess a model's ability to correctly classify positive and negative examples across various threshold values. AUC specifically measures the area under the ROC curve, which plots the true positive rate (TPR) against the false positive rate (FPR). The formula for AUC is:

$$\text{AUC} = \int_0^1 \text{TPR}(f) \, d\text{FPR}(f) \tag{5}$$

Where TPR is the True Positive Rate, and FPR is the False Positive Rate. A higher AUC score indicates a better-performing model, as it signifies that the model is more adept at distinguishing between the positive and negative classes.

We conducted two distinct experiments, as illustrated in Fig. 9, to evaluate the performance of different methods in our facial expression recognition task. In the first experiment, we implemented the LFP algorithm in combination with a neural network architecture, aiming to extract key features from the input images and leverage these features to improve model performance. The LFP algorithm is specifically designed to identify the most relevant pixel groups within the images, which are then processed by the neural network for further analysis. In contrast, the second experiment used max pooling, a more traditional approach, to reduce the spatial dimensions of the input features while retaining the most important information.

The results of these experiments are summarized in Table 1, which clearly demonstrate the superior performance of the LFP algorithm in terms of classification precision. Specifically, the LFP-based model achieved significantly higher precision, indicating that it was more effective in correctly identifying positive instances without misclassifying negative examples as positive. This highlights the strength of the LFP algorithm, particularly in enhancing the accuracy of the model's predictions by focusing on the most relevant features in the image.
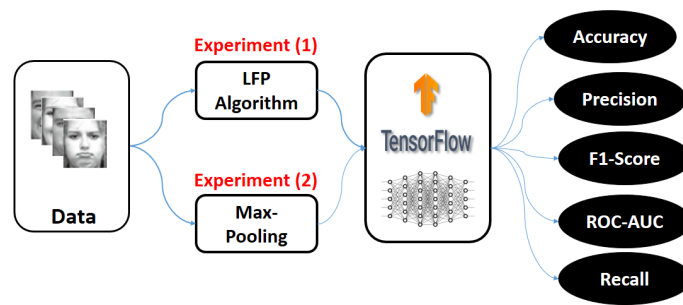
Fig. 9. Training the Neural Network Using Key Features Selected by the LFP Algorithm

Furthermore, when comparing the results from the two experiments, we observed a noticeable improvement in classification accuracy when the LFP algorithm was used. The accuracy of the model in the first experiment, where the LFP algorithm was implemented, was higher by up to 10% compared to the second experiment, which used only max pooling. This suggests that incorporating the LFP algorithm into the neural network pipeline not only improves the precision of predictions but also leads to a more accurate overall classification performance, providing a clear advantage over traditional methods like max pooling [57].

The results presented in Table 1 demonstrate the superior performance of the LFP Algorithm compared to Max Pooling across all five key evaluation metrics: Accuracy, Precision, Recall, F1 Score, and AUC. Specifically, the LFP Algorithm achieved an Accuracy of 0.931, outperforming Max Pooling, which achieved 0.826, representing a significant improvement of 10.5%. In terms of Precision, the LFP Algorithm recorded 0.931, while Max Pooling had a precision of 0.826, indicating a better relevance in positive predictions with the LFP Algorithm. Similarly, for Recall, the LFP Algorithm achieved 0.930, surpassing Max Pooling's 0.825, showcasing better identification of all relevant instances. The F1 Score for the LFP Algorithm was 0.930, compared to 0.824 for Max Pooling, highlighting a more balanced performance in terms of both precision and recall. Finally, in terms of AUC (Area Under the Curve), the LFP Algorithm reached an impressive 0.944, while Max Pooling achieved 0.835, indicating superior model discrimination between positive and negative classes with the LFP Algorithm. The LFP Algorithm outperforms Max Pooling in facial expression recognition, showing up to a 10.5% improvement in Accuracy. It excels in Precision, Recall, and F1 Score, offering a balanced trade-off, and achieves an AUC of 0.944, indicating better class discrimination. These results confirm the LFP Algorithm as a more effective method for improving recognition performance.

Table 1. Comparison of model performance: LFP algorithm vs. max pooling

Method	Accuracy	Precision	Recall	F1 Score	AUC
LFP Algorithm	0.931	0.931	0.930	0.930	0.944
Max Pooling	0.826	0.826	0.825	0.824	0.835

Although the LFP algorithm requires time to identify the coordinates of essential pixel patches, once this step is completed, the selection process during training or testing is significantly faster than Max-Pooling. Unlike Max-Pooling, which recalculates with each data input, the LFP Selector divides the image and directly retrieves the relevant patches based on the coordinates, streamlining the process. This key advantage of LFP over other methods is crucial for improving both efficiency and speed.

Finally, in this study, we utilized the widely recognized "Facial Expression Recognition 2013 (FER2013)" dataset to demonstrate the effectiveness of the LFP algorithm. While our approach showed promising results, it remains somewhat limited in real-world applications due to several fac-

tors. These include challenges such as image quality, which can vary depending on factors like lighting, resolution, and facial positioning, as well as the quality of the internet connection, which can affect the speed and accuracy of data transmission and processing. These limitations highlight the need for further refinement and optimization of the system before it can be effectively deployed in practical scenarios. Nonetheless, our findings underscore the potential of the LFP algorithm, offering a solid foundation for future improvements in emotion recognition.

4. Conclusion

This work demonstrates the effectiveness of the LFP Algorithm in classifying emotions through facial expressions, enhancing personalized learning in our E-learning project. We explored its use in modifying CNN architectures by replacing max and average pooling layers. In experiments, the LFP Algorithm outperformed alternatives, achieving a 0.931 accuracy—10% higher than other methods. After showcasing the LFP algorithm's performance, our next step is to acquire images from real meetings to assemble the best data and retrain our model. Additionally, we plan to create another solution for meetings using the APIs of Google Meet, Microsoft Teams, and Zoom, aligning with our vision. The promising results suggest that further advancements in machine learning could boost emotional recognition and improve E-learning systems.

References

[1] W. A. D. Strasse, D. P. Campos, J. Mendes, C. J. A. Mendonça, J. F. Soni and P. Nohama, "Image Acquisition Protocol by Infrared Medical Thermography in Diaphyseal Tibial Injuries in a Patient Diagnosed with Pseudarthrosis – A Case Study," *2021 Global Medical Engineering Physics Exchanges/Pan American Health Care Exchanges (GMEPE/PAHCE)*, pp. 1-4, 2021, https://doi.org/10.1109/GMEPE/PAHCE50215.2021.9434847.

[2] S. Pan *et al*., "Land-cover classification of multispectral LiDAR data using CNN with optimized hyperparameters," *ISPRS Journal of Photogrammetry and Remote Sensing*, vol. 166, pp. 241–254, 2020, https://doi.org/10.1016/j.isprsjprs.2020.05.022.

[3] R. B. Mancilla, C. Daul, J. G. Martinez, L. L. Salas, D. Wolf, and A. V. Hernandez, "A Quantitative Method for the Detection of Temperature Differences on the Sole of the Foot in Diabetic Patients," in *2021 Global Medical Engineering Physics Exchanges/Pan American Health Care Exchanges (GMEPE/PAHCE)*, pp. 1–5, 2021, https://doi.org/10.1109/GMEPE/PAHCE50215.2021.9434852.

[4] R. Bayareh Mancilla, C. Daul, J. Gutierrez Martinez, A. Vera Hernandez, D. Wolf, and L. Leija Salas, "Detection of Sore-risk Regions on the Foot Sole with Digital Image Processing and Passive Thermography in Diabetic Patients," in *2020 17th International Conference on Electrical Engineering, Computing Science and Automatic Control (CCE)*, pp. 1–6, 2020, https://doi.org/10.1109/CCE50788.2020.9299144.

[5] C. B. Goncalves, J. R. Souza, and H. Fernandes, "Classification of static infrared images using pre-trained CNN for breast cancer detection," in *2021 IEEE 34th International Symposium on Computer-Based Medical Systems (CBMS)*, pp. 101–106, 2021, https://doi.org/10.1109/CBMS52027.2021.00094.

[6] K. Rassels and P. French, "Accurate Body Temperature Measurement of a Neonate Using Thermography Technology," in *2021 Smart Systems Integration (SSI)*, pp. 1–5, 2021, https://doi.org/10.1109/SSI52265.2021.9467024.

[7] M. A. Farooq and P. Corcoran, "Infrared Imaging for Human Thermography and Breast Tumor Classification using Thermal Images," in *2020 31st Irish Signals and Systems Conference (ISSC)*, pp. 1–6, 2020, https://doi.org/10.1109/ISSC49989.2020.9180164.

[8] Y. Dang, C. Benzaïd, B. Yang, T. Taleb and Y. Shen, "Deep-Ensemble-Learning-Based GPS Spoofing Detection for Cellular-Connected UAVs," in *IEEE Internet of Things Journal*, vol. 9, no. 24, pp. 25068-25085, 2022, https://doi.org/10.1109/JIOT.2022.3195320.

[9] P. Rajadanuraks, S. Suranuntchai, S. Pechprasarn, and T. Treebupachatsakul, "Performance Comparison for Different Neural Network Architectures for Chest X-Ray Image Classification," in *2021 7th International Conference on Engineering, Applied Sciences and Technology (ICEAST)*, pp. 49–53, 2021, https://doi.org/10.1109/ICEAST52143.2021.9426289.

[10] M. B. Bora, D. Daimary, K. Amitab, and D. Kandar, "Handwritten Character Recognition from Images using CNN-ECOC," *Procedia Computer Science*, vol. 167, pp. 2403–2409, 2020, https://doi.org/10.1016/j.procs.2020.03.293.

[11] A. M. Fangoh and S. Selim, "Using CNN-XGBoost Deep Networks for COVID-19 Detection in Chest X-ray Images," in *2020 15th International Conference on Computer Engineering and Systems (ICCES)*, pp. 1–7, 2020, https://doi.org/10.1109/ICCES51560.2020.9334600.

[12] N. Nafi'iyah and E. Setyati, "Lung X-Ray Image Enhancement to Identify Pneumonia with CNN," in *2021 3rd East Indonesia Conference on Computer and Information Technology (EIConCIT)*, pp. 421–426, 2021, https://doi.org/10.1109/EIConCIT50028.2021.9431856.

[13] P. Naveen and B. Diwan, "Pre-trained VGG-16 with CNN Architecture to Classify X-Rays Images into Normal or Pneumonia," in *2021 International Conference on Emerging Smart Computing and Informatics (ESCI)*, pp. 102–105, 2021, https://doi.org/10.1109/ESCI50559.2021.9396997.

[14] Y. Ge *et al.*, "Enhancing the X-Ray Differential Phase Contrast Image Quality With Deep Learning Technique," in *IEEE Transactions on Biomedical Engineering*, vol. 68, no. 6, pp. 1751-1758, 2021, https://doi.org/10.1109/TBME.2020.3011119.

[15] G. Labhane, R. Pansare, S. Maheshwari, R. Tiwari, and A. Shukla, "Detection of Pediatric Pneumonia from Chest X-Ray Images using CNN and Transfer Learning," in *2020 3rd International Conference on Emerging Technologies in Computer Engineering: Machine Learning and Internet of Things (ICETCE)*, pp. 85–92, 2020, https://doi.org/10.1109/ICETCE48199.2020.9091755.

[16] Y. Luo, S. Majoe, J. Kui, H. Qi, K. Pushparajah and K. Rhode, "Ultra-Dense Denoising Network: Application to Cardiac Catheter-Based X-Ray Procedures," in *IEEE Transactions on Biomedical Engineering*, vol. 68, no. 9, pp. 2626-2636, 2021, https://doi.org/10.1109/TBME.2020.3041571.

[17] S. Tewari, U. Agrawal, S. Verma, S. Kumar, and S. Jeevaraj, "Ensemble Model for COVID-19 Detection from Chest X-ray Scans using Image Segmentation, Fuzzy Color and Stacking Approaches," in *2020 IEEE 4th Conference on Information & Communication Technology (CICT)*, pp. 1–6, 2020, https://doi.org/10.1109/CICT51604.2020.9312076.

[18] G. Aparna, S. Gowri, R. Bharathi, V. J. S, J. J and A. P, "COVID-19 Prediction using X-Ray Images," *2021 5th International Conference on Trends in Electronics and Informatics (ICOEI)*, pp. 903-908, 2021, https://doi.org/10.1109/ICOEI51242.2021.9452740.

[19] T. Hassan, M. Bettayeb, S. Akcay, S. Khan, M. Bennamoun, and N. Werghi, "Detecting Prohibited Items in X-Ray Images: A Contour Proposal Learning Approach," in *2020 IEEE International Conference on Image Processing (ICIP)*, pp. 2016–2020, 2020, https://doi.org/10.1109/ICIP40778.2020.9190711.

[20] İ. Güven and F. Şimşir, "Demand Forecasting with Color Parameter in Retail Apparel Industry Using Artificial Neural Networks (ANN) and Support Vector Machines (SVM) Methods," *Computers & Industrial Engineering*, vol. 147, p. 106678, 2020, https://doi.org/10.1016/j.cie.2020.106678.

[21] S. H. G. Silva *et al.*, "Soil Texture Prediction in Tropical Soils: A Portable X-Ray Fluorescence Spectrometry Approach," *Geoderma*, vol. 362, p. 114136, 2020, https://doi.org/10.1016/j.geoderma.2019.114136.

[22] S. Parveen and K. B. Khan, "Detection and Classification of Pneumonia in Chest X-ray Images by Supervised Learning," in *2020 IEEE 23rd International Multitopic Conference (INMIC)*, pp. 1–5, 2020, https://doi.org/10.1109/INMIC50486.2020.9318118.

[23] Y. Dang, C. Benzaid, B. Yang, T. Taleb, and Y. Shen, "DeepEnsemble-Learning-Based GPS Spoofing Detection for Cellular-Connected UAVs," *IEEE Internet of Things Journal*, vol. 9, no. 24, pp. 25068–25085, 2022, https://doi.org/10.1109/JIOT.2022.3195320.

[24] P. Rajadanuraks, S. Suranuntchai, S. Pechprasarn, and T. Treebupachatsakul, "Performance Comparison for Different Neural Network Architectures for chest X-Ray Image Classification," in *2021 7th International Conference on Engineering, Applied Sciences and Technology (ICEAST)*, pp. 49–53, 2021, https://doi.org/10.1109/ICEAST52143.2021.9426289.

[25] M. B. Bora, D. Daimary, K. Amitab, and D. Kandar, "Handwritten Character Recognition from Images using CNN-ECOC," *Procedia Computer Science*, vol. 167, pp. 2403–2409, 2020, https://doi.org/10.1016/j.procs.2020.03.293.

[26] A. M. Fangoh and S. Selim, "Using CNN-XGBoost Deep Networks for COVID-19 Detection in Chest X-ray Images," in *2020 15th International Conference on Computer Engineering and Systems (ICCES)*, pp. 1–7, 2020, https://doi.org/10.1109/ICCES51560.2020.9334600.

[27] N. Nafi'iyah and E. Setyati, "Lung X-Ray Image Enhancement to Identify Pneumonia with CNN," in *2021 3rd East Indonesia Conference on Computer and Information Technology (EIConCIT)*, pp. 421–426, 2021, https://doi.org/10.1109/EIConCIT50028.2021.9431856.

[28] P. Naveen and B. Diwan, "Pre-trained VGG-16 with CNN Architecture to classify X-Rays images into Normal or Pneumonia," in *2021 International Conference on Emerging Smart Computing and Informatics (ESCI)*, pp. 102–105, 2021, https://doi.org/10.1109/ESCI50559.2021.9396997.

[29] Y. Ge *et al.*, "Enhancing the X-Ray Differential Phase Contrast Image Quality With Deep Learning Technique," *IEEE Transactions on Biomedical Engineering*, vol. 68, no. 6, pp. 1751–1758, 2021, https://doi.org/10.1109/TBME.2020.3011119.

[30] G. Labhane, R. Pansare, S. Maheshwari, R. Tiwari, and A. Shukla, "Detection of Pediatric Pneumonia from Chest X-Ray Images using CNN and Transfer Learning," in *2020 3rd International Conference on Emerging Technologies in Computer Engineering: Machine Learning and Internet of Things (ICETCE)*, pp. 85–92, 2020, https://doi.org/10.1109/ICETCE48199.2020.9091755.

[31] Y. Luo, S. Majoe, J. Kui, H. Qi, K. Pushparajah, and K. Rhode, "Ultra-Dense Denoising Network: Application to Cardiac Catheter-Based X-Ray Procedures," *IEEE Transactions on Biomedical Engineering*, vol. 68, no. 9, pp. 2626–2636, 2021, https://doi.org/10.1109/TBME.2020.3041571.

[32] S. Tewari, U. Agrawal, S. Verma, S. Kumar, and S. Jeevaraj, "Ensemble Model for COVID-19 detection from chest X-ray Scans using Image Segmentation, Fuzzy Color and Stacking Approaches," in *2020 IEEE 4th Conference on Information & Communication Technology (CICT)*, pp. 1–6, 2020, https://doi.org/10.1109/CICT51604.2020.9312076.

[33] G. Aparna, S. Gowri, R. Bharathi, V. J. S, J. J, and A. P, "COVID-19 Prediction using X-Ray Images," in *2021 5th International Conference on Trends in Electronics and Informatics (ICOEI)*, pp. 903–908, 2021, https://doi.org/10.1109/ICOEI51242.2021.9452740.

[34] T. Hassan, M. Bettayeb, S. Akcay, S. Khan, M. Bennamoun, and N. Werghi, "Detecting Prohibited Items in X-Ray Images: a Contour Proposal Learning Approach," in *2020 IEEE International Conference on Image Processing (ICIP)*, pp. 2016–2020, 2020, https://doi.org/10.1109/ICIP40778.2020.9190711.

[35] İ. Güven and F. Şimşir, "Demand forecasting with color parameter in retail apparel industry using artificial neural networks (ANN) and support vector machines (SVM) methods," *Computers & Industrial Engineering*, vol. 147, p. 106678, 2020, https://doi.org/10.1016/j.cie.2020.106678.

[36] S. H. G. Silva *et al.*, "Soil texture prediction in tropical soils: A portable X-ray fluorescence spectrometry approach," *Geoderma*, vol. 362, p. 114136, 2020, https://doi.org/10.1016/j.geoderma.2019.114136.

[37] S. Parveen and K. B. Khan, "Detection and classification of pneumonia in chest X-ray images by supervised learning," in *2020 IEEE 23rd International Multitopic Conference (INMIC)*, pp. 1–5, 2020, https://doi.org/10.1109/INMIC50486.2020.9318118.

[38] Z. Mei, K. Ivanov, G. Zhao, Y. Wu, M. Liu, and L. Wang, "Foot type classification using sensor-enabled footwear and 1D-CNN," *Measurement*, vol. 165, p. 108184, 2020, https://doi.org/10.1016/j.measurement.2020.108184.

[39] J. Bonnard, K. Abdelouahab, M. Pelcat, and F. Berry, "On building a CNN-based multi-view smart camera for real-time object detection," *Microprocessors and Microsystems*, vol. 77, p. 103177, 2020, https://doi.org/10.1016/j.micpro.2020.103177.

[40] L. M. Schliephake, I. Trempler, M. A. Roehe, N. Heins, and R. I. Schubotz, "Positive and negative prediction error signals to violated expectations of face and place stimuli distinctively activate FFA and PPA," *NeuroImage*, vol. 236, p. 118028, 2021, https://doi.org/10.1016/j.neuroimage.2021.118028.

[41] A. M. Muir, A. C. Eberhard, M. S. Walker, A. Bennion, M. South, and M. J. Larson, "Dissociating the effect of reward uncertainty and timing uncertainty on neural indices of reward prediction errors: A reward positivity (RewP) event-related potential (ERP) study," *Biological Psychology*, vol. 163, p. 108121, 2021, https://doi.org/10.1016/j.biopsycho.2021.108121.

[42] V. N. Almeida, "Neurophysiological basis of the N400 deflection, from Mismatch Negativity to Semantic Prediction Potentials and late positive components," *International Journal of Psychophysiology*, vol. 166, pp. 134–150, 2021, https://doi.org/10.1016/j.ijpsycho.2021.06.001.

[43] E. Rawls and C. Lamm, "The aversion positivity: Mediofrontal cortical potentials reflect parametric aversive prediction errors and drive behavioral modification following negative reinforcement," *Cortex*, vol. 140, pp. 26–39, 2021, https://doi.org/10.1016/j.cortex.2021.03.012.

[44] S. E. Mansour, A. Sakhi, L. Kzaz, O. Tali, and A. Sekkaki, "Focal Point of Learning," in *2021 IEEE 12th Annual Ubiquitous Computing, Electronics & Mobile Communication Conference (UEMCON)*, pp. 0522–0526, 2021, https://doi.org/10.1109/UEMCON53757.2021.9666524.

[45] A. Sakhi, S.-E. Mansour, A. Sekkaki, and K. Benzidane, "The Use of the AI to Classify the Emotion Intelligence (EI) Students," in *2022 IEEE 13th Annual Information Technology, Electronics and Mobile Communication Conference (IEMCON)*, pp. 0148–0152, 2022, https://doi.org/10.1109/IEMCON56893.2022.9946581.

[46] S. E. Mansour, A. Sakhi, L. Kzaz, A. Erroutbi, and A. Sekkaki, "Electronic device for acquiring images of sardine cans," in *2022 IEEE World AI IoT Congress (AIIoT)*, pp. 471–475, 2022, https://doi.org/10.1109/AIIoT54504.2022.9817260.

[47] S. Eddine Mansour, A. Sakhi, L. Kzaz, O. Tali, and A. Sekkaki, "Design, security and implementation of learning focal point algorithm in a docker container," *IJEECS*, vol. 33, no. 1, p. 416, 2024, https://doi.org/10.11591/ijeecs.v33.i1.pp416-424.

[48] S.-E. Mansour, A. Sakhi, L. Kzaz, and A. Sekkaki, "Enhancing Security Mechanisms for IoT-Fog Networks," *Journal of Robotics and Control*, vol. 5, no. 1, pp. 152–159, 2024, https://doi.org/10.18196/jrc.v5i1.20745.

[49] A. Sakhi, S.-E. Mansour, and A. Sekkaki, "Using Learning Focal Point Algorithm to Classify Emotional Intelligence," *Journal of Robotics and Control*, vol. 5, no. 1, pp. 263–270, 2024, https://doi.org/10.18196/jrc.v5i1.20895.

[50] S. E. Mansour, A. Sakhi, L. Kzaz, and A. Sekkaki, "Leveraging the learning focal point algorithm for emotional intelligence," *International Journal of Reconfigurable and Embedded Systems (IJRES)*, vol. 13, no. 3, p. 767, 2024, https://doi.org/10.11591/ijres.v13.i3.pp767-773.

[51] S. E. Mansour, A. Sakhi, "Detection of Sealing Defects in Canned Sardines Using Local Binary Pattern and Perceptron Techniques for Enhanced Quality Control," *International Journal of Robotics and Control Systems*, vol. 5, no. 1, p. 585, 2025, https://doi.org/10.31763/ijrcs.v5i1.1737.pp585-598

[52] S. E. Mansour, A. Sakhi, "Leveraging LFP Architecture for Pneumothorax Detection in Chest X-rays," *Journal of Robotics and Control*, vol. 6, no. 1, pp. 336–344, 2025, https://doi.org/10.18196/jrc.v6i1.25107.

[53] M. M. Odeh *et al.*, "A prediction model of risk factors for complications among SARS-CoV2 positive patients: Cases from Jordan," *Journal of Infection and Public Health*, vol. 14, no. 6, pp. 689–695, 2021, https://doi.org/10.1016/j.jiph.2021.02.010.

[54] A. Sonawat, H.-M. Yang, and J.-H. Kim, "Experimental study of positive displacement hydraulic turbine at various temperatures and development of empirical co-relation for flowrate prediction," *Renewable Energy*, vol. 172, pp. 1293–1300, 2021, https://doi.org/10.1016/j.renene.2021.03.118.

[55] Y. Ochi *et al.*, "Validation of the Kumamoto criteria for prediction of 99m technetium pyrophosphate scintigraphy positivity as a strategy for diagnosis of transthyretin cardiac amyloidosis: A retrospective cohort study in Kochi," *Journal of Cardiology*, vol. 77, no. 2, pp. 124–130, 2021, https://doi.org/10.1016/j.jjcc.2020.06.019.

[56] D. L. Pinto *et al.*, "Image feature extraction via local binary patterns for marbling score classification in beef cattle using tree-based algorithms," *Livestock Science*, vol. 267, p. 105152, 2023, https://doi.org/10.1016/j.livsci.2022.105152.

[57] N. Guillou and G. Chapalain, "Machine learning methods applied to sea level predictions in the upper part of a tidal estuary," *Oceanologia*, vol. 63, no. 4, pp. 531–544, 2021, https://doi.org/10.1016/j.oceano.2021.07.003.